LANGMUIR

Interfaces: Adsorption, Reactions, Films, Forces, Measurement Techniques, Charge Transfer, Electrochemistry, Electrocatalysis, Energy Production and Storage

In situ Study of Layer by Layer Polyelectrolyte Deposition in Nanopores of Anodic Aluminum Oxide by Reflectometric Interference Spectroscopy

Imad Zamrik, Haider Bayat, Qasim Alhusaini, Mohammad Raoufi, and Holger Schönherr

Langmuir, **Just Accepted Manuscript** • DOI: 10.1021/acs.langmuir.9b03769 • Publication Date (Web): 01 Feb 2020

In situ Study of Layer by Layer Polyelectrolyte Deposition in Nanopores of Anodic Aluminum Oxide by Reflectometric Interference Spectroscopy

*Imad Zamrik,[1#] Haider Bayat,[1#] Qasim Alhusaini,[1] Mohammad Raoufi,[1,2] and Holger Schönherr,[1]**

[1] Physical Chemistry I, Department of Chemistry and Biology & Research Center of Micro and Nanochemistry and Engineering (*Cμ*), University of Siegen, Siegen, Germany

[2] Department of Pharmaceutical Biomaterials and Medical Biomaterials Research Center, Faculty of Pharmacy, Tehran University of Medical Sciences, Tehran, Iran

* Corresponding Author: Prof. Dr. Holger Schönherr

Email: schoenherr@chemie.uni-siegen.de, Tel.: (+49) 271 - 740 2806

# Both authors contributed equally.

KEYWORDS: Anodic aluminum oxide, nanopores, confinement, layer by layer polyelectrolyte deposition, reflectometric interference spectroscopy.

ABSTRACT

The modification of cylindrical anodic aluminum oxide (AAO) nanopores by alternating layer by layer (LBL) deposition of poly(sodium-4-styrene sulfonate) (PSS) and poly(allylamine hydrochloride) (PAH) was studied *in situ* by Reflectometric Interference Spectroscopy (RIfS). In particular, the kinetics of polyelectrolyte deposition inside the 37 ± 3 nm diameter and 3.7 ± 0.2 μm long pores was unraveled and potential differences in LBL multilayer growth compared to flat silicon substrates and the effect of different ionic strengths and different types of ions were investigated. RIfS measures the effective optical thicknesses, which is for constant pore length proportional to the effective refractive index of the AAO sample, from which in turn the deposited mass of polymer or the corresponding layer thickness can be estimated. Compared to the multilayer growth by LBL deposition on flat amino-silane primed silicon wafers, which was assessed by spectroscopic ellipsometry, the thickness increment per deposited bilayer as well as the dependence of this increment on ionic strength (0.01 to 0.15) and counter ion type (Na^+ vs. Ca^{2+}) inside the amino-silane primed nanopores was for the first bilayers to within the experimental error identical. For thicker multilayers, the pore diameter became smaller, which led to reduced thickness increments and eventually virtually completely filled pores. The observed kinetics is consistent with a mass transport limited adsorption of the polyelectrolyte to the charged surface according to a Langmuir isotherm with negligible desorption rate. In addition to fundamental insight into the build-up of polyelectrolyte multilayers inside AAO nanopores, our results highlight the sensitivity of RIfS and its use as analytical tool for probing processes inside nanopores and for the development of biosensors.

Introduction

Label-free biosensors have attracted increasing attention in the medical field[1] as well as for environmental monitoring [2] and applications in biochemically-oriented research.[3] The main principle of label-free biosensors comprises the combination of an analyte of interest with a specific material that possesses e.g. an optical,[4] acoustic,[5] or electrochemical[6] response, which can be later converted to a readable and comparable signal.[7] In this context the application of nanoporous sensor interfaces has been discussed to enhance the signal by increased internal surface area and also exploitation of special optical effects. Among the prime examples is the detection of relevant enzymes, which may be used to signal the presence of certain pathogens.[8,9]

Among the various detection methods, reflectometric interference spectroscopy (RIfS)[10] has shown is potential in combination with nanoporous sensor interfaces.[11] In general, RIfS is a well-established method that is based on the interference of the white light at two (semi)transparent interfaces and it has attracted particular attention due to its simplicity and convenience of use for thick film samples.[12] As RIfS is a very sensitive technique, it was utilized in many studies including surface profiling,[13,14] metrology,[15] optical and chemical biosensors,[16] refractive index measurements for thin films,[17] and many other.[18,19,20, 21] RIfS relies on the change in average index of refraction of the dielectric between the two (semi)transparent interfaces, and its utility can be enhanced by exploiting the increased internal surface area, e.g. inside a nanoporous substrate, in which the thickness of the porous layer L is fixed.[22] The deposition of a material inside the nanopores increases the effective refractive index of the medium (n_e) yielding a higher effective optical thickness (EOT) in the interference pattern measured in the

optical spectrum.[23] The analysis of the acquired reflectance spectra enables in addition to the determination of the thickness of a deposited layer within the nanopores also the *in situ* monitoring the kinetics of the deposition in the liquid phase[24] according to the Fabry-Pérot effect described by the following equation:[25]

Equation 1 $$EOT = 2n_e L \cos\theta$$

where *EOT* is the effective optical thickness of the thin film, n_e is its effective refractive index, L is its physical thickness of the thin film, and θ is the incidence angle of light.

In this context, nanoporous substrates, such as AAO, have been considered attractive, since they can be utilized without the necessity of cumbersome substrate preparation like for instance required for optical waveguide spectroscopy (OWS) For OWS it is necessary to remove the metallic Al at the backside and to mount the AAO membrane onto a glass slides using an optical adhesive.[26] Compared to porous silicon, AAO nanopores were reported to possess superior physical and chemical properties for label free chemical and biological sensing.[27] In addition, the pore cross section is circular and can be tailored by the parameters of the anodization process.

The layer-by-layer (LbL) assembly of polyelectrolytes[28] inside nanoporous structures received tremendous attention for the fabrication of nanostructured objects,[29,30,31,32] resulting in controllable modification with precisely defined layers of soft materials.[33,34]

The LbL multilayer fabrication approach is very versatile, and lends itself for nanostructures fabrication and modification for many potential applications in different areas, such as free standing nanotubes,[30,31,32,35,36,37,38] chemical sensors,[39] photodiodes,[40] nonlinear optics,[41] optical devices,[42] drug delivery,[43,44] food[45] and the biomedical field.[46,47] A typical example of applying LbL approach in biosensing was reported in a previous work,[22] where the kinetics of the adsorption of DNA on PAH functionalized surfaces of flat and porous substrateswas studied. Thus, the investigation of the parameters that can influence the deposition of biological and naturally occurring polyelectrolytes, such as proteins and DNA, have highlighted the importance to study the difference in the deposition behavior of the polyelectrolytes by applying variable parameters.

In previous studies, the LbL process inside AAO nanopores was investigated by OWS and it was shown that the pore diameter affects the LbL process.[48] It was also reported that severely increasing confinement occurs after reducing the pore diameter by adsorbed polyelectrolytes during the LBL deposition.[49] On the other hand, the adsorption of polymer close to the AAO pore orifice and its effect on the LBL process inside the membrane as well as the suppression of this detrimental process indicate that many details have to be considered for LBL inside nanopores. In particular the kinetics of the process and the dependence on ionic strength and counter ion type remain open questions.

PSS and PAH, as benchmark polyelectrolytes, were reported to form very stable multilayers with a low polyelectrolyte mobility.[50] In addition, they have been the constituents of LBL replicas of AAO nanopores that afforded free standing open

nanotubes.[30,35] Here, we reported on the modification of AAO nanopores by alternating deposition of PSS and PAH. The deposition of the polyelectrolytes was studied *in situ* by RIfS for different ionic strengths and salt types to unravel the effects of these factors and to determine whether or not confinement effects are important.

Experimental:

Materials: Aluminum (99.9999%, 0.5 mm thick plate, Chempure), poly(allylamine hydrochloride) (C.N. 71550-12-4, M_w = 120,000 − 200,000 g/mol, Alfa Aesar), poly(sodium styrenesulfonate) (C.N. 25704-18-1, M_w = 70,000 g/mol, Sigma-Aldrich), 3-(ethoxydimethylsilyl)propylamine (97%, C.N. 18306-79-1, Sigma-Aldrich), phosphoric acid (C.N. 7664-38-2, 85%, Chemische Fabrik Budenheim,), oxalic acid (C.N. 6153-56-6, Merck), perchloric acid (C.N. 7601-90-3, 60−62%, J.T. Baker), Milli-Q water (from a Millipore Direct-Q 8 system with resistivity of 18.0 MΩ cm, Millipore, Schwalbach, Germany), KOH (C.N. 1310-58-3, Roth), NaCl (C.N. 7647-14-5, Baker), $CaCl_2 \cdot 6\ H_2O$ (C.N. 7774-34-7, Sigma Aldrich), chromium oxide (C.N. 27081-50G-F, Sigma-Aldrich), HCl (C.N. 7647-01, 37%, VWR), H_2O_2 (C.N. CAS 7722-84-1, 30%, Roth), concentrated sulfuric acid (C.N. 7664-93-9 95%, Chemsolute)) and silicon (100) wafers (P/Boron type, manufactured by OKMETIC, Finland) were purchased from the suppliers listed.

RIfS. The interferometric reflectance spectra of AAO were collected by using a CCD detector (USB 2000+) equipped with a tungsten halogen light source (LS-1) attached to a bifurcated optical probe (R400-7-VIS/NIR) (all purchased from Jaz, Ocean Optics, Inc., Dunedin, FL, USA). The tungsten lamp transfers the light to the optical probe and the

reflected light is collected by the same probe and transferred to the CCD detector. The reflectivity data were recorded in the wavelength range of 400-1000 nm.

The interference pattern recorded was analyzed by Fourier transformation (utilizing wave metrics IGOR Pro 6 and Fringes 22.6 data analysis software) of the reflectance spectrum. The resulting peak position corresponds to the value of *EOT* of the thin film. The refractive index of the porous alumina was considered to be 1.77.[51,52]

Flow cell: The homebuilt tetragonal flow cell made of stainless steel has the following dimension: 30 mm × 30 mm × 20 mm. The upper side of the cell possesses a hole with a transparent quartz cap to allow the light to pass through to the sample, which is fixed at the bottom of the cell. A rubber O-ring (Wilhelm Jung GmbH) was used on the backside of the AAO template and on the front side of the transparent cap to seal the compartments (Figure S1, Supporting Information)

Scanning Electron Microscopy (SEM) Measurements. The SEM data were acquired on a Zeiss Ultra 55cv field emission scanning electron microscope (FESEM) (Zeiss, Oberkochen, Germany). All measurements were performed with an operation voltage of 10 kV with the Inlens secondary electron detector. For the analysis of the FESEM micrographs, SPIP software (scanning probe image processor, Version 5.0.7) was used.

Preparation of AAO nanopores. Nanoporous AAO was prepared by a two-step anodization process using 0.3 M oxalic acid as electrolyte at 15°C and 40 V, as previously described, by two-step anodization.[35] The first anodization was performed for 18 h, followed by chemical etching of the obtained pores by a treatment in an aqueous mixture of chromic acid (1.8 wt %) and phosphoric acid (6 wt %) for 4 h at 63°C. The

second anodization was executed for 30 min to obtain nanopores, open on one end only, with 3.7 ± 0.3 μm length and 37 ± 3 nm diameter, according to SEM analysis (see Figure S2, Supporting Information).

LbL polyelectrolyte deposition. For the flat substrates, 2 cm × 1 cm pieces of a silicon wafer were cleaned by treatment with piranha solution (70/30 mixture by volume of concentrated sulfuric acid and hydrogen peroxide) for 2 min, followed by rinsing with copious amounts of Milli-Q water (Caution: piranha solution should be handled with extreme caution! It has been reported to detonate unexpectedly.) The nanoporous AAO samples were sonicated in Milli-Q water three times for 10 min before they were dried in vacuum for 1 h. Both the AAO and silicon samples together with one drop of 3-(ethoxydimethylsilyl)propylamine were kept in a desiccator at a pressure of 16 mbar at room temperature for 24 h to obtain a monolayer of the aminosilane. All of AAO templates were then coated with a thin Au film by sputtering ~10 nm gold (Edwards Sputter Coater S150B) at 15 - 20 × 10^{-1} mm Hg to afford a passivation primer layer that (*i*) prevents the build-up of polyelectrolyte multilayers on top of the AAO template[35] and (*ii*) to increase as a semi-transparent mirror the reflectivity of the substrates, which affords a significant improvement of the RIfS signal.

For LBL deposition on the flat substrates, the cleaned silicon wafers were immersed consecutively into solutions of PSS (concentration 0.5 g/L in 0.15 M NaCl in Milli-Q water), Milli-Q water, PAH (concentration 0.5 g/L in 0.15 M NaCl in Milli-Q water), and again Milli-Q water. The previous process was repeated using solutions of PSS (0.5 g/L in 0.01 M NaCl in Milli-Q water), PAH (0.5 g/L in 0.01 M NaCl in Milli-Q water), PSS (0.5 g/L in 0.05 M $CaCl_2$ in Milli-Q water), PAH (0.5 g/L in 0.05 M $CaCl_2$ in Milli-

Q water). Dipping times in polyelectrolyte solutions were 20 min; the washing step in Milli-Q water lasted for 10 min. The adsorption and rinsing steps were repeated as required. After the deposition of the desired number of polyelectrolyte layers, the samples were dried in a stream of nitrogen. The previous process was emulated using the AAO samples and the flow cell: Milli-Q water was pumped through the cell at first for each AAO sample for 10 minutes. The corresponding RIfS measurement was considered as a baseline or reference starting *EOT* value. This was followed by introducing the polyelectrolyte solutions into the chamber with a constant flow rate of 1.6 mL min^{-1} to deposit polyelectrolyte layers, similar to the procedure described for flat Si substrates above. The RIfS data were captured continuously and were analyzed as mentioned above.

Results and Discussion

AAO fabrication

For the *in situ* study of the LbL deposition of polyelectrolyte multilayers inside AAO, AAO samples prepared by two subsequent anodization steps were used. The cross-sectional and top view SEM micrographs in Figure 22 show a length *L* of 3.7 ± 0.3 μm and regular hexagonally ordered AAO nanopores with a dimeter of 37 ± 3 nm (SI Figure 3). The pore diameters were calculated by analyzing pore areas observed in the SEM images utilizing ImageJ open source image processing program, which equates the corresponding size of an equivalent spherical pore.

After the functionalization, the AAO substrate, the aminosilane primed AAO was then sputter-coated under an angle of 45° with a thin Au film. This film functions according to previous work[355] as a passivation layer that prevents polyelectrolyte multilayers from adsorbing stably at the surface of the template. It also serves to improve the reflectivity of the top surface in RIfS to obtain higher amplitudes and more pronounced Fabry-Perot fringes.

RIfS applied to deposition of polyelectrolyte layers inside AAO nanopores

The polyelectrolyte deposition in the AAO nanopores was investigated *in situ* by RIfS. Reflectance spectra (Figure 1a) were recorded continuously. From the spectra recorded the *EOT* values were estimated from the fast Fourier transform (FFT) (inset Figure 1a). The corresponding values of *ΔEOT*, estimated as the difference with respect to the value of *EOT* of the baseline, were then plotted as a function of time (Figure 1b). The results obtained were compared to values acquired on flat silicon wafers by variable angle spectroscopic ellipsometry (*vide infra*). In particular, LBL deposition on flat vs. nanoporous substrates, the kinetics, the multilayer buildup vs. pore size and the effects of ionic strength and cation type were systematically investigated.

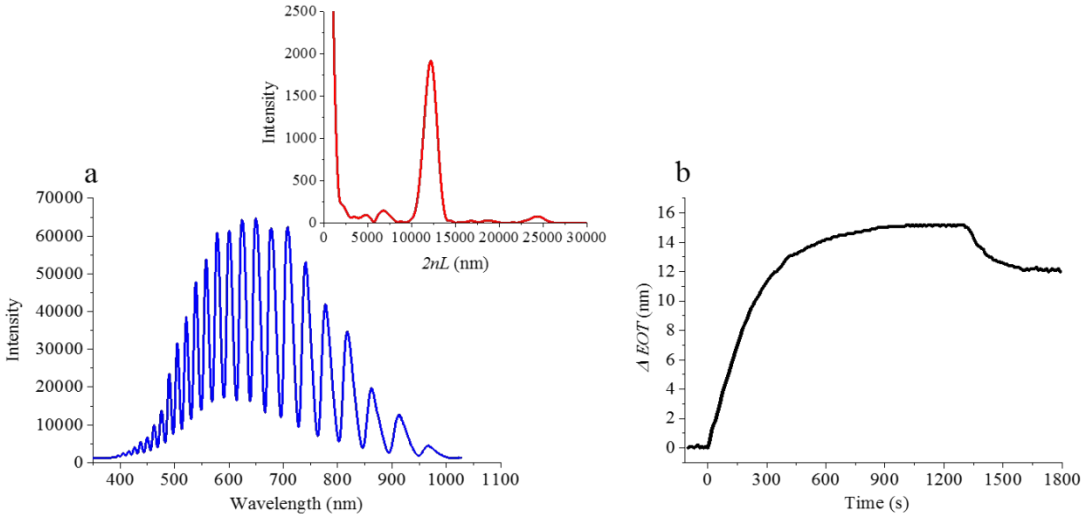

Figure 1. (a) Reflectance spectrum recorded by RIfS for the kinetic of PSS layer deposition inside AAO nanopores (pore length L = 3.7 ± 0.3 µm, pore diameter of 37 ± 3 nm), the inset shows the corresponding FFT; (b) RIfS time lapse data for both adsorption (at time zero) and rinsing (after ~ 1350 s) processes.

LBL on flat silicon vs LBL inside AAO nanopores

The polyelectrolyte multilayer thickness was found to increase linearly with the number of deposited bilayers both on flat Si (Figure 2a) and inside AAO (Figure 2b) for both applied ionic strengths, indicating a stepwise and regular deposition process.

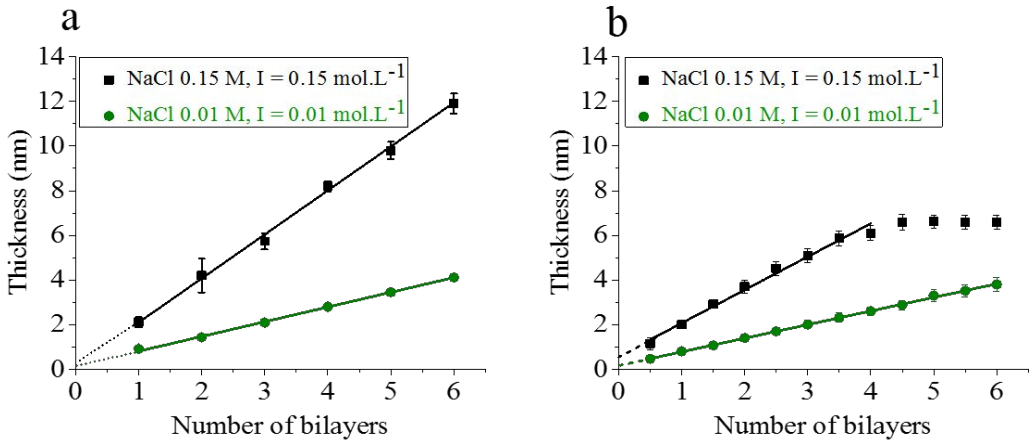

Figure 2. (a) Ellipsometric film thickness determined in the dry state of (PSS/PAH) multilayers deposited on aminosilane-primed silicon substrates at two different ionic strengths (0.15 and 0.01) as a function of the number of the deposited bilayers. (b) Thickness values determined from *in situ* measurements of *ΔEOT* by RIfS of $(PSS/PAH)_n$ multilayers deposited in silanized AAO substrates at two different ionic strengths (0.15 and 0.01) as a function of the number of the deposited bilayers (for a plot of *ΔEOT* compare Figure S3). The blue and green lines correspond to linear least square fits in panel (b) the last three data points with constant thickness value were not considered. The error bars were calculated as standard deviation (n = 3). The coefficients of determination for both linear fits are $R^2 > 0.99$.

Consequently, a variation of the pore diameter and pore length (Figure S4, Supporting Information) corroborates the above interpretation, showing that a doubled pore diameter and a doubled pore length lead to similar deposited polymer mass in 0.15 M NaCl.

For flat Si, the thickness increment per bilayer for lower ionic strength buffer solutions was smaller than for higher ionic strength buffer solutions. The total film thickness of 6 bilayers was 12.3 nm in the 0.15 M NaCl solution, while only 3.5 nm was obtained in the case of 0.01 M NaCl. Similar results were reported in previous work at ionic strengths in the range between 1 - 2 M NaCl and PSS with M_w = 100 kg/mol and PAH with M_w = 50-65 kg/mol.[53] Adjusting the ionic strength does not change the charge density along the polymer chain for strong polyelectrolytes, but instead changes the effectiveness of repulsion or attraction due to charged groups in close proximity due to charge screening. The increasing concentration of mobile ions increases the screening of the charged groups along the chain from each other and decreases the distance over which they can repel each other, as described by the Debye length.

On Si, the thickness of the multilayers increased linearly with the number of adsorbed bilayers. The intercepts of the linear fits refer to the thickness of primer layer of 3-(ethoxydimethylsilyl)propylamine, which was found to be 0.18 ± 0.04 nm and 0.26 ± 0.04 nm for high and low ionic strength, respectively. These values are compatible with previous work performed on silicon dioxide, where the reported thickness was 0.11 nm.[54]

In the AAO nanopores, the assembly of PAH/PSS multilayers was investigated using RIfS. Similar to the ellipsometry data for flat Si substrates presented in Figure 2a, the LbL deposition in the AAO nanochannels shows initially a linear growth (Figure 2b). The mass deposition in terms of ΔEOT at higher ionic strength was also higher than at lower ionic strength. This result is qualitatively in agreement with previous work performed on AAO substrates at comparable conditions (PSS with M_w = 150 g/mol and PAH with M_w = 70 g/mol).[55] The higher ionic strength led also to a lower number of

deposited bilayers before the pores were effectively blocked; only 4.5 bilayers could be deposited, whereas 6 bilayers were deposited in the low ionic strength case, before the thickness increment was negligible.

The chains of the polyelectrolyte in multilayers assembled at low salt concentration can be expected to be oriented flat and more parallel to the substrates, while at higher salt concentration the chains were more coiled, which led to thicker coils adsorbed at the interface. A higher salt concentration is also known to lead to more entangled polymer and weaker repulsion causing a larger thickness formation.

The number of deposited bilayers in LbL in nanopores was reported to be limited, which is related to the initial diameter of the pores.[47] As the bilayers deposited at higher ionic strength have considerably higher thickness due to increased effective size of the coils,[56] fewer bilayers could be deposited in 0.15 M NaCl due to the onset of hindered diffusion within the nanopores near the pore entrance. By contrast, 0.01 M NaCl allowed more material to be deposited, i.e. more layers, as the mass deposition was less per bilayer than 0.15 NaCl.

The thickness increment for different ionic strength on AAO substrate was calculated from the acquired RIfS spectra applying the two component Maxwell-Garnett equation[57]

Equation 2
$$n_e^2 = n_{Al_2O_3}^2 \frac{2n_{Al_2O_3}^2 + n_{void}^2 + 2P\left(n_{void}^2 - n_{Al_2O_3}^2\right)}{2n_{Al_2O_3}^2 + n_{void}^2 - P\left(n_{void}^2 - n_{Al_2O_3}^2\right)}$$

where $n_{Al_2O_3}$ is the constant refractive index of the bulk AAO ($n_{Al_2O_3}$ = 1.70 in this work), n_{void} is the refractive index of the material filled or deposited in the pores, and P is the porosity of the AAO pores, which can be calculated according to the pore diameter and the inter pores distance,

and the Lorentz-Lorenz equation (see also Table 1)[58]

Equation 3
$$\frac{n_v^2-1}{n_v^2+2} = f_1\frac{n_1^2-1}{n_1^2+2} + f_2\frac{n_2^2-1}{n_2^2+2}$$

where n_v is the refractive index of the void medium inside pores (calculated from the acquired RIfS spectra applying the equation 2, n_1 is the refractive index of the Milli-Q water, n_2 is the refractive index of the PSS/PAH bilayer (n_2 = 1.50) [59], f_1 and f_2 are the volume fractions of Milli-Q water and the deposited bilayer respectively.

As it is shown in Tables 1 and 2, the initially deposited bilayers inside the AAO nanopores were found to possess almost the same deposited mass (in terms of thicknesses). The deposited bilayers thicknesses in AAO were estimated according to each of the calculated values of n_v, applying (eq. 2) and the values of f_2 applying (eq. 3), where f_1=1-f_2. For more than 3 to 4 bilayers the deposition is increasingly hindered and reduced mass deposition was observed. While similar thicknesses were observed here for deposition on flat Si and inside AAO, Lee et al reported larger thickness increments for

nanopores at the pore orifice.[60] The data determined here by RIfS average the deposited mass over the entire pore length and hence yields a mean thickness, unlike e.g. microscopy data acquired at the pore opening.

Table 1. LBL multilayer thickness from ellipsometry and thickness from RIfS for deposition from 0.15 M NaCl.

Bilayer Number	Thickness on Si wafer (nm)	Thickness in AAO nanopores (nm)
1	2.1 ± 0.2	2.0 ± 0.2
2	4.2 ± 0.8	3.7 ± 0.3
3	5.7 ± 0.4	5.1 ± 0.3
4	8.2 ± 0.2	6.2 ± 0.3

Table 2. LBL multilayer thickness from ellipsometry and thickness from RIfS for deposition from 0.01 M NaCl.

Bilayer Number	Thickness on Si wafer (nm)	Thickness in AAO nanopores (nm)
1	0.91 ± 0.06	0.8 ± 0.1
2	1.43 ± 0.06	1.4 ± 0.2
3	2.09 ± 0.03	2.0 ± 0.2
4	2.80 ± 0.04	2.6 ± 0.2
5	3.45 ± 0.01	3.3 ± 0.3
6	4.11 ± 0.02	3.8 ± 0.3

The same initial thickness increment could be thus observed both on flat and in nanoporous substrates, i.e. the LbL deposition inside the nanopores occurs in a similar manner compared to the one on the flat substrate as well as the reduction in the

thicknesses per bilayer for both substrates, when applying polyelectrolyte solutions with lower ionic strength. This result was confirmed in Table 3 by comparing the ratios of the slopes of the linear sections of the plots in Figures 4a and 4b on both substrates. The values of 2.85 ± 0.08 and 2.48 ± 0.113 are to within the uncertainty identical. The uncertainties were estimated via error propagation.

The somewhat lower than expected bilayers thickness in the increasingly narrow nanochannels can be attributed to the buildup of a diffusion barrier as well as a depletion of unabsorbed polyelectrolyte within the channel albeit probably to a lower extent. Depletion of polyelectrolytes confined between two charged surfaces has been predicted by Böhmer *et al.*[61] using self-consistent field simulations. According to Böhmer *et al.,* for small gaps at low salt concentrations, which result in low charge screening, the adsorption of polyanions onto positively pre-charged surface causes a negative potential throughout the channel. As a result, the flux of polyanions into the nanochannel is reduced due to this negative potential, leading to a lower polyanion concentration within the nanochannel, and in consequence, hindering further adsorption. The Debye length depends significantly on the ionic strength of the polymer solution. When the Debye length is large relative to the channel width, significant depletion of polyelectrolyte within the channel is predicted. The Debye lengths for the NaCl concentrations of 0.15 and 0.01 M used in our study are 0.78 and 3.0 nm, respectively, therefore, no pronounced effect of electrical double layers overlapping is expected in the LBL coated AAO substrates.

Table 3. Thickness increments per bilayer for deposition from buffer solutions with different ionic strength on flat Si substrate and inside AAO nanopores.

Ionic strength	Flat substrate [nm]	Ratio of the slopes	AAO nanopores [nm]	Ratio of the slopes
0.15M	1.97 ± 0.05	2.85 ± 0.08	1.49 ± 0.06	2.48 ± 0.11
0.01M	0.66 ± 0.01		0.60 ± 0.01	

Effect of the type of counter ion

Since the adsorption is discussed in terms of ion exchange,[62] it is expected that different ions with differing affinity may change the surface excess of adsorbed polyelectrolytes. In LbL, complexes are formed between inorganic counterions and the polyelectrolyte molecules, where the high electrostatic polyelectrolyte potential causes nearly all counterions to form complexes with charged monomers. The final result of this ion bridge phenomenon is a stronger polymer chain contraction and a comparatively smaller deposited thickness of the polyelectrolyte.[63] However, it was reported that the ionic strength is more important for the structure and thickness of the adsorbed layer than the valence of the counterions in solutions of low ionic strength ($I \leq 0.2$).[64]

The effect of the counter cation type on the LBL deposition process was studied here at constant ionic strength (I = 0.15). In the experiments aqueous solution with concentrations of 0.15 M NaCl and 0.05 M $CaCl_2$, respectively, were applied. The

deposition was performed on the same types of silane-primed substrates as discussed above.

Figure 3a shows the effect of the counter cation type in the buffer solution on the LbL deposition on a flat substrate, while Figure 3b shows the corresponding data for AAO. For flat Si, the data show a linear bilayer thickness increment for LBL deposition from solutions of both salts, but a lower mass deposition for $CaCl_{2c}$. Similar results were reported in previous work at constant ionic strength of I = 1.0 and PSS with M_w = 70 g/mol and PAH with M_w = 70 g/mol. [65] In that work, the thickness of the multilayer films was reduced from 97.5 ± 2.2 nm to 93.5 ± 4.0 nm, when the 1 M NaCl buffer solution was altered by replacing part of NaCl with $MgCl_2$ (0.85 M NaCl / 0.05 M $MgCl_2$ buffer solution at constant ionic strength of 1.0 was applied). The intercepts acquired in the linear fits in Figure 3 refer to the thickness of the primer layer of 3-(ethoxydimethylsilyl)propylamine, which was found to be 0.19 ± 0.04 and 0.13 ± 0.04 for the experiments with $CaCl_2$ and NaCl containing solutions, respectively.

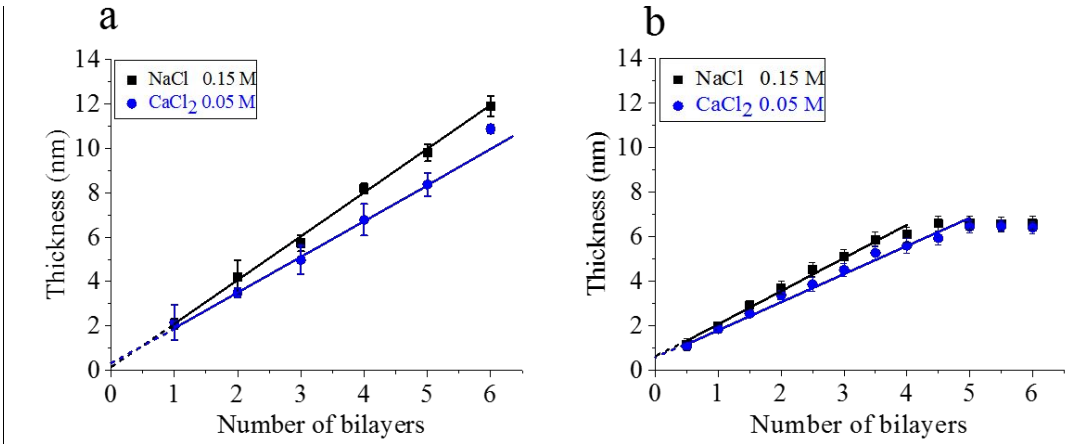

Figure 3. (a) Film thickness (dry thickness) determined by ellipsometry of (PSS/PAH) multilayers deposited on aminosilane-primed silicon substrates at the same ionic strength

(0.15) and two different counterions (0.15 M NaCl solution vs. 0.05 M $CaCl_2$ solution) as a function of the number of the deposited bilayers. (b) Thickness values determined from *in situ* measurements of *ΔEOT* by RIfS of $(PSS/PAH)_n$ multilayers deposited in silanized AAO substrates at the same ionic strength (0.15M) and two different counterions (0.15 M NaCl solution vs. 0.05 M $CaCl_2$ solution) as a function of the number of the deposited bilayers (for a plot of *ΔEOT* compare Figure S3).. The blue and black lines correspond to linear least square fits; in panel (b) the last two data points with constant thickness value were not considered. The error bars were calculated as standard deviation (n = 3). The coefficients of determination for both linear fits are $R^2 > 0.99$.

For AAO, similar results were obtained. The LbL assembly in nanochannels showed initially linear growth (Figure 3b). The lower shift also in the *ΔEOT* values in case of $CaCl_2$ compared to NaCl indicates at this condition a lower mass deposition and less bilayer thickness inside the AAO nanopores took place. This may be attributed to the stronger polymer-chain contraction[66] in comparison to NaCl. The pore blocking occurred for 5 bilayers (Figure 3b).

As was shown above in Table 1, the thickness of deposited polyelectrolyte inside the AAO nanopores can be calculated by applying the Lorenz-Lorentz approach (Equ. 3). Accordingly, the corresponding data for the experiments shown above in Figure 3b were analyzed and the results were compared in Table 4 to the data of the experiments of the flat substrate case (Figure 3a).

Table 4. Thickness from ellipsometry and thickness from RIfS of 0.05 M $CaCl_2$.

Thickness by ellipsometry (nm)	Thickness by RIfS (nm)
2.2 ± 0.8	2.0 ± 0.1
3.5 ±0.2	3.7 ± 0.2
5.0 ± 0.6	5.1 ± 0.3
6.8 ± 0.7	6.1 ± 0.3
8.4 ± 0.5	7.0 ± 0.3

Similar mass deposition and polyelectrolyte thickness values were obtained for both substrates, but a slightly lower bilayer thickness in the AAO substrate compared to the flat substrate was observed due to the hindered diffusion and thereby depletion of polyelectrolytes inside the nano-channels. This result was confirmed by the ratio of the slopes. The ratios of the slopes of 1.08 ± 0.04 and 1.18 ± 0.06 are identical to within the uncertainty, which indicates that a very similar deposition process took place on both utilize substrates (Table 5).

Table 5. Thickness increment per bilayer in mono and divalent buffer solutions on flat substrates and AAO nanopores. The uncertainties were estimated via error propagation.

Buffer Solution	Ionic strength	Flat substrate [nm]	Ratio of the slopes	AAO nanopores [nm]	Ratio of the slopes
NaCl	0.15 M	1.97 ± 0.05	1.08 ± 0.04	1.49 ± 0.06	1.18 ± 0.06
$CaCl_2$	0.15 M	1.82 ± 0.05		1.26 ± 0.04	

Kinetics of LbL inside AAO

In the LbL process, the rate of polyelectrolyte deposition is proportional to the polyelectrolyte concentration and to the fraction of unoccupied surface area or in analogy to the number of unoccupied binding sites on the surface. Adsorption of polyelectrolyte molecules will continue and the surface excess will increase over time until it plateaus.

It can be shown that the ΔEOT vs. time can be described by the following equation:[67]

Equation 4 $$\Delta EOT_t = \frac{k_{on}[A]\Delta EOT_{max}}{k_{on}[A] + k_{off}}\left(1 - e^{-k_{obs}t}\right)$$

where $[A]$ is the polyelectrolyte concentration, k_{on} is the apparent association rate constant in units of M^{-1} s^{-1}, and k_{off} is the apparent dissociation rate constant in s^{-1}.[68] k_{obs} is the observed rate constant (s^{-1}), and t is the time (s).

k_{obs} can be expressed as:[69]

Equation 5 $$k_{obs} = k_{on}c - k_{off}$$

where c is the polyelectrolyte concentration (M).

Since the functionalized AAO walls essentially act as a reacting surface (perfect sink),[70] a stationary concentration profile results that renders the adsorption entirely controlled by mass transport into the nanopores.

Typical kinetics traces of the LbL process of PSS layer deposition inside the AAO nanopores are shown in the Figure 4 for low and high ionic strength in NaCl solutions as well as for $CaCl_2$ solutions.

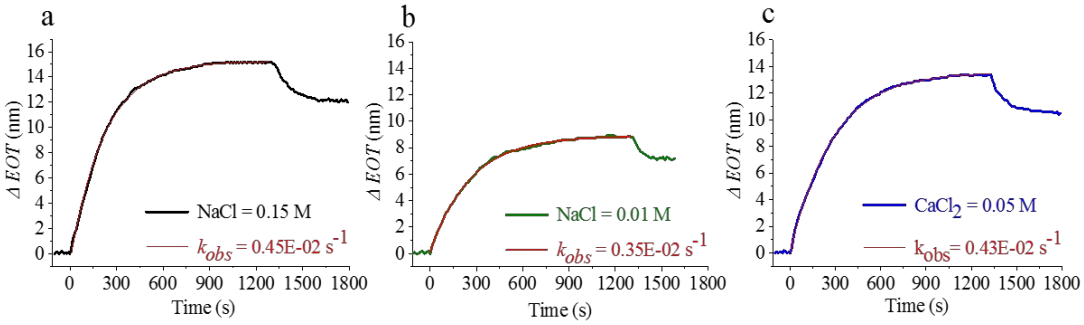

Figure 4. Adsorption kinetics of PSS onto AAO nanopores: NaCl solutions with ionic strengths of (a) 0.15 and (b) 0.01 as well as (c) $CaCl_2$ solution with an ionic strength of 0.15. All transient data were fitted to equation 4 to afford values for k_{obs}.

When the PSS solution was flushed into the flow cell, the value of ΔEOT increased as the PSS solution replaced the Milli-Q water and the polyanions molecules adsorbed on the inner walls. With increasing surface excess of PSS, the film thickness increased until it reached the saturation value. Washing with Milli-Q water reduced the value of ΔEOT in both solutions due to the replacement of the void medium and desorption of loosely physisorbed PSS molecules. The continuous slow increase to ΔEOT_{max} hence is

explained by the further adsorption of polyelectrolyte molecules on the AAO surface. The decrease in ΔEOT after reaching ΔEOT_{max} also is primarily due to the replacement of the polyelectrolyte solution by Milli-Q water and a very minor desorption of the loosely bonded polyelectrolytes molecules. A higher value for k_{obs} (0.0045 s^{-1}) was observed for the high ionic strength NaCl solution, while a lower value for k_{obs} (0.0035 s^{-1}) for the lower ionic strength was obtained. The data for CaCl (k_{obs} = 0.0043 s^{-1}) was similar to the high ionic strength NaCl solution.

The change of the void medium represents only a minor contribution to the observed ΔEOT, considering the refractive index of applied polyelectrolytes solutions to be 1.3343 and 1.3350 for 0.01 M and 0.15 M NaCl solutions, respectively, and 1.3347 for 0.05 M $CaCl_2$ (measured by an Abbé refractometer). The Milli-Q water replacement with polyelectrolyte solutions thus caused an almost instant shift in ΔEOT (≈ 10% of ΔEOT).

Effect of polyelectrolyte concentration

The polyelectrolyte concentration was reported to have a negligible effect on the multilayer thickness and increment in LBL. [71] To confirm these literature data and to investigate in how far this also holds inside AAO, four concentrations were varied at constant ionic strength of 0.15 (NaCl). The deposition kinetics is shown in Figure 5a. According to Equations 4 and 5, the rate at which the system equilibrates depends not only on k_{on} and c, but also on k_{off}. The affinity of the polyelectrolyte molecule to the charged group on the surface is related to the k_{off} value, which can be estimated from the analysis of a plot of k_{obs} vs c (Figure 5b).

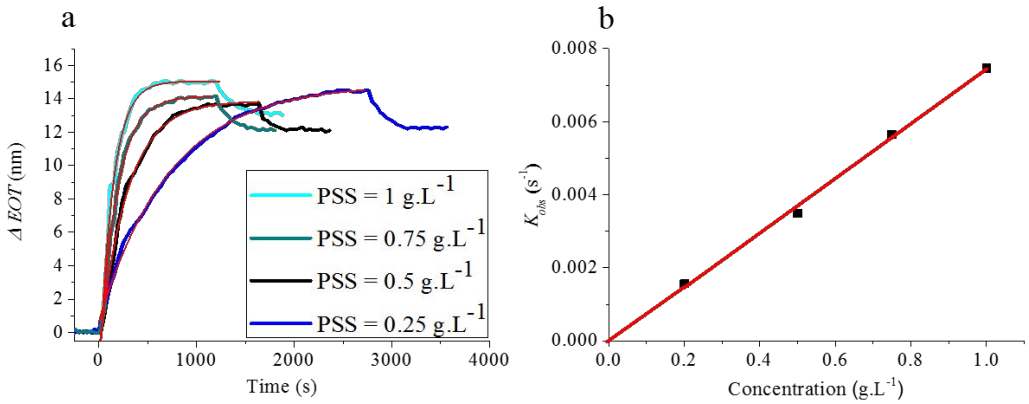

Figure 5. (a) Adsorption kinetics of different PSS concentration diluted in 0.15 M NaCl. (b) Plot of k_{obs} values vs. PSS concentrations. The red line corresponds to a linear least squares fit of the data.

It can be seen in Figure 5a that all PSS deposition kinetics plateaued at similar EOT_{max} values, which confirms that the polyelectrolyte concentration has a negligible effect on the mass deposition in LbL deposition. By fitting the acquired kinetics of each applied concentration to the equation 5 (Figure 5b), a linear relation between the k_{obs} values and the applied concentration was observed. This observation agrees with the expected dependence that the apparent rate of adsorption scales linearly with polymer concentration. From the intercept ($4 \times 10^{-5} \pm 2 \times 10^{-6}$ s^{-1}) a very tight binding and irreversible adsorption of the polyelectrolyte molecules can be concluded. The overall results are consistent with a mass transport limited adsorption of the polyelectrolyte to the charged surface according to a Langmuir isotherm with negligible k_{off}.

Conclusions

The alternating LBL deposition of PSS and PAH inside aminosilane monolayer modified AAO nanopores with 37 ± 3 nm diameter results in deposited layer thicknesses that are for the first layers to within the uncertainty identical to the deposition on similarly aminosilane primed flat Si substrates. As unveiled by *in situ* Reflectometric Interference Spectroscopy the effect of different ionic strengths (0.15 vs. 0.01) and different types of cations (Na^+ vs Ca^{2+}) was also very similar, implying negligible confinement effects, which is in line with the values of the Debye lengths of 0.78 and 3.0 nm. The polyelectrolyte deposition resulted in stepwise deceasing pore diameter, which led to reduced mass of deposited polyelectrolyte per adsorption step. The observed kinetics is consistent with a mass transport limited adsorption of the polyelectrolyte to the charged surface according to a Langmuir isotherm with negligible desorption rate.

ASSOCIATED CONTENT

Supporting Information

Schematic of flow cell; SEM data of nanopores, values of ΔEOT vs. number of bilayers, Reflectometry data for LBL deposition in AAO with varied pore dimensions.

AUTHOR INFORMATION

Corresponding Author

*Email: schoenherr@chemie.uni-siegen.de

Author Contributions

The manuscript was written through contributions of all authors. All authors have given approval to the final version of the manuscript

Notes

The authors declare no competing financial interest.

Acknowledgment

The authors gratefully acknowledge Dr. Sergey I. Druzhinin and Dr. Daniel Wesner for inspiring discussions, Prof. Dr. Xin Jiang for access to the FESEM, Professor Michael J. Sailor, University of California, for kindly providing the reflectometry analysis software, and Dr. Marc Steuber for acquiring some of the SEM data. Part of this work was performed at the Micro- and Nanoanalytics Facility (MNaF) at the University of Siegen. The authors gratefully acknowledge funding by the German Academic Exchange

Service, DAAD (Ph.D. stipends to HB and QA) and the University of Siegen (incl. a research grant of the School and Science and Technology).

ToC Graphics

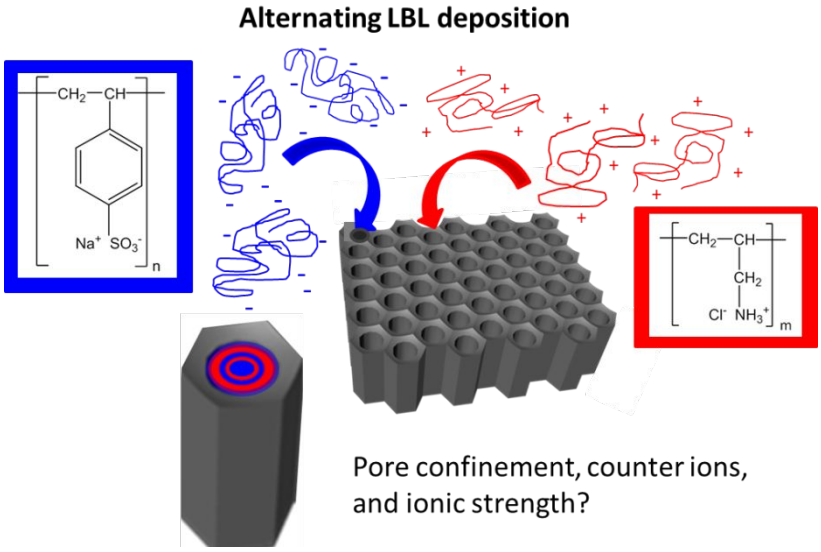

References

(1) Malhotra, B. D.; Chaubey, A. Biosensors for clinical diagnostics industry. *Sensors and Actuators B: Chemical.* **2003,** *91*, 117–127.

(2) González-Martínez, M. A.; Puchades, R.; Maquieira, A. Optical immunosensors for environmental monitoring: How far have we come? *Anal. Bioanal. Chem.* **2007**, *387*, 205–218.

(3) Fägerstam, L. G.; Frostell-Karlsson, Å.; Karlsson, R.; Persson, B.; Rönnberg, I. Biospecific interaction analysis using surface plasmon resonance detection applied to kinetic, binding site and concentration analysis. *Journal of Chromatography A* **1992**, *597*, 397–410.

(4) Gauglitz, G. Direct optical sensors: principles and selected applications. *Anal Bioanal Chem*. **2005,** *381*, 141–155.

(5) Länge, K.; Rapp, B.; Rapp, M. Surface acoustic wave biosensors: a review. *Anal. Bioanal. Chem*. **2008**, *391*, 1509– 1519.

(6) Grieshaber, D.; MacKenzie, R.; Voros, J.; Reimhult, E. Electrochemical Biosensors - Sensor Principles and Architectures. *Electrochemical Biosensors*. **2008**, *8*, 1400– 1458.

(7) Rajeev, G.; Xifre-Perez, E.; Prieto Simon, B.; Cowin, A. J.; Marsal, L. F.; Voelcker, N. H. A label-free optical biosensor based on nanoporous anodic alumina for tumour necrosis factor-alpha detection in chronic wounds. *Sensors & Actuators, B: Chemical* **2018**, *257*, 116–123.

(8) M. Nemati, Abel Santos, T. Kumeria, D. Losic. Label-Free Real-Time Quantification of Enzyme Levels by Interferometric Spectroscopy Combined with Gelatin-Modified Nanoporous Anodic Alumina Photonic Films. *Anal. Chem*. **2015**, 87, 9016−9024.

(9) M. Amouzadeh Tabrizi, J. Ferré-Borrull, L. F. Marsal. Highly sensitive IRS based biosensor for the determination of cytochrome c as a cancer marker by using nanoporous anodic alumina modified with trypsin. *Biosensors and Bioelectronics*, **2020**, 149, 111828.

(10) Brecht, A.; Gauglitz, G.; Nahm, W. Interferometric measurements used in chemical and biochemical sensors, *Analysis. Analysis*. **1992**, *20*, 135– 140.

(11) Krismastuti, F. S. H.; Bayat, H.; Voelcker, N. H.; Schönherr, H. Real Time Monitoring of Layer-by-Layer Polyelectrolyte Deposition and Bacterial Enzyme Detection in Nanoporous Anodized Aluminum Oxide. *Anal. Chem.***2015,** *8*7, 3856–3863.

(12) Hirth, F.; Buck, T. C.; Grassi, A. P.; Koch, A. W. Depth-sensitive thin film reflectometer. *Meas. Sci. Technol.* **2010**, *21*, 125301.

(13) Debnath, S. K.; You, J.; Kim, S.-W. Determination of film thickness and surface profile using reflectometry and spectrally resolved phase shifting interferometry. *Int. J. Precis. Eng. Manuf.* **2009**, *10*, 5–10.

(14) Madani-Grasset, F.; Pham, N. T.; Glynos, E.; Koutsos, V. Imaging thin and ultrathin organic films by scanning white light interferometry. *Mater. Sci. Eng. B* **2008**, *152*, 125–131.

(15) Maniscalco, B.; Kaminski, P. M.; Walls, J. M. Thin film thickness measurements using Scanning White Light Interferometry. *Thin Solid Films* **2014**, *550*, 10–16.

(16) Brecht, A.; Piehler, J.; Lang, G.; Gauglitz, G. A direct optical immunosensor for atrazine detection. *Anal. Chim. Acta.* **1995**, *311*, 289–299.

(17) Buron, C.; Membrey, F.; Filiâtre, C.; Foissy, A. A new approach to determine the mean thickness and refractive index of polyelectrolyte multilayer using optical reflectometry. *Colloids Surf. A Physicochem. Eng. Asp*. **2006**, *289*, 163–171.

(18) Carter, M. C. D.; Sorrell, C. D.; Serpe, M. J. J. Deswelling Kinetics of Color Tunable Poly(*N*-Isopropylacrylamide) Microgel-Based Etalons. *Phys. Chem. B* **2011**, *115*, 14359–14368.

(19) Jiang, M.; Gerhard, E. A simple strain sensor using a thin film as a low-finesse fiber-optic Fabry–Perot interferometer. *Sens. Actuators A Phys.* **2001**, *88*, 41–46.

(20) Kaur, S.; Law, C. S.; Williamson, N. H.; Kempson, I.; Popat, A.; Kumeria, T.; Santos, A. Environmental Copper Sensor Based on Polyethylenimine-Functionalized Nanoporous Anodic Alumina Interferometers. *Anal. Chem* **2019**, *91*, 5011–5020.

(21) Kim, D.-K.; Kerman, K.; Saito, M.; Sathuluri, R. R.; Endo, T.; Yamamura, S.; Kwon, Y.-S.; Tamiya, E. Label-Free DNA Biosensor Based on Localized Surface Plasmon Resonance Coupled with Interferometry. *Anal. Chem.* **2007**, *79*, 1855–1864.

(22) Ihmels, H.; Jiang, S.; Mahmoud, M. M. A.; Schönherr, H.; Wesner, D.; Zamrik, I. Fluorimetric Detection of G-Quadruplex DNA in Solution and Adsorbed on Surfaces with a Selective Trinuclear Cyanine Dye. *Langmuir* **2018**, *34*, 11866–11877.

(23) Alvarez, S. D.; Li, C.-P.; Chiang, C. E.; Schuller, I. K.; Sailor, M. J. A label-free porous alumina interferometric immunosensor. *ACS Nano* **2009,** *3*, 3301–3307.

(24) Nemati, M.; Santos, A.; Losic, D. Fabrication and Optimization of Bilayered Nanoporous Anodic Alumina Structures as Multi-Point Interferometric Sensing Platform. *Sensors* **2018**, *18*, 470.

(25) Kuncser, C.; Kuncser, A.; Antohe, S. Optical path difference behind of spectacular game of light. *Procedia Soc. Behav. Sci.* **2011**, *15*, 2890–2896.

(26) Lazzara, T. D.; Lau, K. H. A.; Knoll, W. J. Mounted Nanoporous Anodic Alumina Thin Films as Planar Optical Waveguides. *Nanosci. Nanotechnol*. **2010**, *10*, 4293–4299.

(27) Kumeria, T.; Santos, A.; Losic, D. Nanoporous Anodic Alumina Platforms: Engineered Surface Chemistry and Structure for Optical Sensing Applications. *Sensors* **2014,** *14*, 11878–11918.

(28) Decher, G. Fuzzy Nanoassemblies: Toward Layered Polymeric Multicomposites. *Science* **1997**, *277*, 1232–1237.

(29) Ariga, K.; Hill, J. P.; Ji, Q. Layer-by-layer assembly as a versatile bottom-up nanofabrication technique for exploratory research and realistic application. *Phys. Chem. Chem. Phys.* **2007**, *9*, 2319- 2340

(30) Ai, S. F.; Lu, G.; He, Q.; Li, J. B. Highly flexible polyelectrolyte nanotubes. *J. Am. Chem. Soc.* **2003**, *125*, 11140−11141.

(31) Roy, C. J.; Dupont-Gillain, C.; Demoustier-Champagne, S.; Jonas, A. M.; Landoulsi, J. Growth Mechanism of Con fined Polyelectrolyte Multilayers in Nanoporous Templates. *Langmuir* **2010**, *26*, 3350−3355.

(32) Cho, Y.; Lee, W.; Jhon, Y. K.; Genzer, J.; Char, K. Polymer Nanotubules Obtained by Layer-by-Layer Deposition Within AAO Membrane Templates with Sub-100-nm Pore Diameters. *Small* **2010**, *6*, 2683−2689.

(33) Seyrek, E.; Decher, G. Layer-by-Layer Assembly of Multifunctional Hybrid Materials and Nanoscale Devices. *Polymer Science* **2012**; 159–185.

(34) Azzaroni, O.; Lau, K. H. A. Layer-by-layer assemblies in nanoporous templates: nano-organized design and applications of soft nanotechnology. *Soft Matter* **2011,** *7*, 8709-8724

(35) Raoufi, M.; Tranchida, D.; Schönherr, H. Pushing the Size Limits in the Replication of Nanopores in Anodized Aluminum Oxide via the Layer-by-Layer Deposition of Polyelectrolytes. *Langmuir* **2012**, 28, 10091–10096.

(36) Raoufi, M.; Schönherr, H. Fabrication of Complex Free-Standing Nanostructures with Concave and Convex Curvature via the Layer-by-Layer Approach *Langmuir* **2014**, *30*, 1723–1728.

(37) Raoufi, M.; Schönherr, H. Improved Synthesis of Anodized Aluminum Oxide with Modulated Pore Diameters for the Fabrication of Polymeric Nanotubes. *RSC Adv.* **2013,** *3,* 13429 - 13436.

(38) Bayat, H.; Lin, C.-H.; Cheng, M.-H.; Steuber, M; Chen, J.-T.; Schönherr, H. Interplay of Template Constraints and Microphase Separation in Polymeric Nanoobjects Replicated from Novel Modulated and Interconnected Nanoporous Anodic Alumina. *ACS Appl. Nano Mater.* **2018,** 1, 200 - 208.

(39) Yang, Y. J.; Jiang, Y. D.; Xu, J. H.; Yu, J. S. Preparation and properties of multilayer poly(3,4-ethylenedioxythiophene) Langmuir–Blodgett film. *Thin Solid Films* **2008**, *516*, 2120-21124.

(40) Eckle, M.; Decher, G. Tuning the Performance of Layer-by-Layer Assembled Organic Light Emitting Diodes by Controlling the Position of Isolating Clay Barrier Sheets. *Nano Lett.* **2001**, *1*, 45-49.

(41) Laschewsky, A.; Mayer, B.; Wischerhoff, E.; Arys, X.; Bertrand, P.; Delcorte, A.; Jonas, A. A new route to thin polymeric, non-centrosymmetric coatings. *Thin Solid Films* **1996**, *285*, 334-337.

(42) Hiller, J.; Mendelsohn, J. D.; Rubner, M. F. Reversibly erasable nanoporous anti-reflection coatings from polyelectrolyte multilayers. *Nat. Mater.* **2002**, *1*, 59-63.

(43) Izumrudov, V. A.; Kharlampieva, E.; Sukhishvili, S. A. Multilayers of a Globular Protein and a Weak Polyacid: Role of Polyacid Ionization in Growth and Decomposition in Salt Solutions. *Biomacromolecules* **2005**, *6*, 1782-1788.

(44) Dongen, S. F. M.; Hoog, H. P. M.; Peters, R.; Nallani, M.; Nolte, R. J. M.; Hest, J. C. M. Biohybrid Polymer Capsules. *Chem. Rev.* **2009**, *109*, 6212.

(45) Guzey, D.; McClements, D. J. Formation, stability and properties of multilayer emulsions for application in the food industry. *Adv. Coll. Interf.* **2006**, *128*, 227–248.

(46) Volodkin, D. V.; Madaboosi, N.; Blacklock, J.; Skirtach, A. G.; Möhwald, H. Surface-Supported Multilayers Decorated with Bio-active Material Aimed at Light-Triggered Drug Delivery. *Langmuir* **2009**, *25*, 14037-14043.

(47) Tang, Z. Y.; Wang, Y.; Podsiadlo, P.; Kotov, N. A. Biomedical Applications of Layer-by-Layer Assembly: From Biomimetics to Tissue Engineering. *Adv. Mater.* **2006**, *18*, 3203.

(48) Lazzara, T. D.; Lau, K. H. A.; Knoll, W.; Janshoff, A.; Steinem, C. Beilstein J. Macromolecular shape and interactions in layer-by-layer assemblies within cylindrical nanopores. *Nanotechnol*. **2012**, *3*, 475–484.

(49) Alem, H.; Blondeau, F.; Glinel, K.; Demoustier-Champagne, S.; Jonas, A. M. Layer-by-Layer Assembly of Polyelectrolytes in Nanopores. *Macromolecules* **2007**, *40*, 3366–3372.

(50) Schmitt, J.; Gruenewald, T.; Decher, G.; Pershan, P. S.; Kjaer, K.; Loesche, M. Internal structure of layer-by-layer adsorbed polyelectrolyte films: a neutron and x-ray reflectivity study. *Macromolecules* **1993**, *26*, 7058–7063.

(51) French, R. H.; Müllejans, H.; Jones, D. J. Determined from Vacuum Ultraviolet and Electron Energy-Loss Spectroscopies. *J. Am. Ceram. Soc.* **1998**, *81*, 2549–2557.

(52) Hohlbein, J.; Rehn, U.; Wehrspohn, R. B. In-situ optical characterisation of porous alumina. *Phys. Stat. Sol.* **2004**, *201*, 803–807.

(53) Decher, G.; Schmitt, J. Fine-Tuning of the film thickness of ultrathin multilayer films composed of consecutively alternating layers of anionic and cationic polyelectrolytes. *Progr. Colloid Polym. Sci.* **1992**, *89*, 160–164.

(54) Zhang, F.; Sautter, K.; Larsen, A. M.; Findley, D. A.; Davis, R. C.; Samha, H.lR. Chemical vapor deposition of three aminosilanes on silicon dioxide. *Langmuir* **2010**, *26*, 14648–14654.

(55) Lazzara, T. D.; Lau, K. H. A.; Abou-Kandil, A. I.; Caminade, A.-M.; Majoral, J.-P.; Knoll, W. Polyelectrolyte Layer-by-Layer Deposition in Cylindrical Nanopores. *ACS Nano* **2010**, *4*, 3909–3920.

(56) Dubas, S. T.; Schlenoff, J. B. Factors Controlling the Growth of Polyelectrolyte Multilayers. *Macromolecules* **1999**, *32*, 8153–8160.

(57) Garnett, J. C. M. Colours in Metal Glasses and in Metallic Films. *Philos. Trans. R. Soc. Lond., B, Biol. Sci.* **1904**, *203*, 385–420.

(58) Born, M. A.; Wolf, E. Principles of Optics: Electromagnetic Theory of Propagation, Interference and Diffraction of Light, 6th ed.; University Press: Cambridge, 1980.

59) Feldötö, Z.; Lundin, M.; Braesch-Andersen, S.; Blomberg, E. Adsorption of IgG on/in a PAH/PSS multilayer film: Layer structure and cell response. *J. Colloid Interface Sci.* **2011**, *354*, 31–37.

(60) Lee, D.; Nolte, A. J.; Kunz, A. L.; Rubner, M. F.; Cohen, R. E. pH-Induced Hysteretic Gating of Track-Etched Polycarbonate Membranes: Swelling/Deswelling Behavior of Polyelectrolyte Multilayers in Confined Geometry. *J. Am. Chem. Soc.* **2006**, *128*, 8521-8529.

(61) Böhmer, M. R.; Evers, O. A.; Scheutjens, J. Weak polyelectrolytes between two surfaces: adsorption and stabilization. *Macromolecules* **1990**, *23*, 2288–2301.

(62) Decher, G. *Polyelectrolyte Multilayers, An Overview*; Wiley Online Books, 2002.

(63) Podgornik, R.; Ličer, M. *Curr. Opin.* Polyelectrolyte bridging interactions between charged macromolecules. *Colloid Interface. Sci.* **2006,** *11*, 273–279.

(64) Dahlgren, M. A.G. Effect of counterion valency and ionic strength on polyelectrolyte adsorption. *Langmuir* **1994**, *10*, 1580–1583.

(65) Dressick, W. J.; Wahl, K. J.; Bassim, N. D.; Stroud, R. M.; Petrovykh, D. Y. Divalent–Anion Salt Effects in Polyelectrolyte Multilayer Depositions. *Langmuir* **2012,** *28*, 15831–15843.

(66) Cho, Y.; Lee, W.; Jhon, Y. K.; Genzer, J.; Char, K. Polymer Nanotubules Obtained by Layer-by-Layer Deposition Within AAO Membrane Templates with Sub-100-nm Pore Diameters. *Small* **2010**, *6*, 2683−2689.

(67) O'Shannessy, D. J.; Brigham-Burke, M.; Soneson, K. K.; Hensley, P.; Brooks, I. Determination of rate and equilibrium binding constants for macromolecular interactions using surface plasmon resonance: use of nonlinear least squares analysis methods. *Analy. Biochem.* **1993**, *212*, 457–468.

(68) Majka J.; Speck C. Advances in Biochemical EngineeringBiotechnology. *Adv. Biochem. Engin. Biotechnol*. **2007,** *104,* 13–36.

(69) Böhm, H.-J.; Klebe, G. What Can We Learn from Molecular Recognition in Protein–Ligand Complexes for the Design of New Drugs. *Angew. Chem. Int. Ed.* **1996**, *35*, 2588–2614.

(70) Lazzara, T. D.; Mey, I.; Steinem, C.; Janshoff, A. Benefits and Limitations of Porous Substrates as Biosensors for Protein Adsorption. *Anal. Chem.* **2011**, *83*, 5624–5630.

(71) Ruths, J.; Essler, F.; Decher, G.; Riegler, H. Polyelectrolytes I: Polyanion/ Polycation Multilayers at the Air/Monolayer/Water Interface as Elements for Quantitative Polymer Adsorption Studies and Preparation of Hetero-superlattices on Solid Surfaces. *Langmuir* **2000,** *16*, 8871–8878.